Negative capacitance in organic light-emitting diodes

L. S. C. Pingree
Department of Materials Science and Engineering, Northwestern University, Evanston, Illinois 60208-3108

B. J. Scott, M. T. Russell, and T. J. Marks
Department of Chemistry, Northwestern University, Evanston, Illinois 60208-3113

M. C. Hersam[a)]
Department of Materials Science and Engineering, Northwestern University, Evanston, Illinois 60208-3108

Negative capacitance has been characterized in organic light-emitting diode (OLED) heterostructures using impedance spectroscopy. Although similar inductive behavior has been previously reported for transient electroluminescence in OLEDs, definitive identification of negative capacitance in impedance spectroscopy data has been elusive due to the high concentration of distributed traps at the anode-organic interface. The addition of a layer of 4,4′-bis[(*p*-trichlorosilylpropylphenyl)phenylamino]-biphenyl at this interface minimizes these trapping sites, thus enabling the inductive nature of charge transport in OLEDs to be directly observable. By quantitatively correlating the resulting impedance spectroscopy data with equivalent circuit models, a detailed description of charge transport in OLEDs as a function of heterostructure composition is developed. © *2005 American Institute of Physics.* [DOI: 10.1063/1.1865346]

Since the introduction of organic light-emitting diodes (OLEDs) to the electronic display market, a number of commercial applications have surfaced.[1] Due to their high efficiency, richness of color, flexibility, ruggedness, and wide thermal operation range, OLEDs are finding uses in small-area consumer product displays, military applications, and emergency response equipment.[1–4] In many display applications, OLEDs respond to a time varying bias as pixels are continuously cycled. Consequently, strategies for optimizing frequency dependent charge transport in OLED displays will likely have broad technological impact.

In previous work, negative capacitance (NC) was identified as an important parameter that influences frequency dependent charge transport in electronic and optoelectronic devices. In components exhibiting NC, the reactance is positive at low frequencies, and the resistance initially increases with frequency. When present, this trend is apparent in the Cole-Cole impedance plot as a region which extends into the fourth quadrant and exhibits the aforementioned increase in resistance as a function of frequency.[5] NC has been previously observed and modeled in Si diodes,[6–9] metal-oxide-semiconductor tunnel diodes,[5] quantum well infrared photodetectors,[10] GaAs *p-i-n* structures,[11] metallic nanoparticles in dielectric matrices,[12] and polymer LEDs.[13,14] In these examples, NC was attributed to bias dependent conductivity modulation, minority carrier flow, slow transient time of injected carriers, or charge trapping.[5–14]

In this letter, impedance spectroscopy is used to characterize previously unreported NC in OLED charge transport measurements, thus demonstrating similar time constants as observed in transient OLED electroluminescence.[15,16] Measurements across a wide bias range illustrate that the onset frequency of NC varies exponentially with the square root of the applied bias in accordance with Poole–Frenkel theory, unlike previous reports on polymer LEDs.[13,14] Through the

generation of equivalent circuit models that fit the experimental data, the frequency dependent charge transport properties are explained as a function of the OLED heterostructure composition.

Experiments were performed on OLEDs with 1.5 mm × 5 mm active areas which were fabricated according to the following procedure. Indium tin oxide (ITO) coated glass slides with a sheet resistance of <30 Ω/cm from Thin Film Devices were cleaned and modified with an interfacial layer of 4,4′-bis[(*p*-trichlorosilylpropylphenyl)phenylamino]-biphenyl (TPD-Si$_2$) according to a procedure reported elsewhere.[17] The hole transport material *N,N′*-di(α-naphthyl)-*N,N′*-diphenyl-1,1′-biphenyl-4,4′-diamine (NPB)[18] and the electron transport/emissive material tris(8-hydroxyquinalato)aluminum (III) (Alq$_3$)[19] (Aldrich, 99.995%) were purified by gradient sublimation. NPB and Alq$_3$ layers were subsequently deposited by thermal evaporation (1.5–2.0 Å/s) to a thickness of 25 and 30 nm, respectively, at previously reported base pressures.[17] The cathodes consisted of 80 nm thick aluminum layers (Aldrich, 99.999%) deposited thermally at 1.5 Å/s. Schematic cross sections of the two OLED structures are shown in the insets of Figs. 1(a) and 1(b).

Impedance spectroscopy measurements were carried out by a HP 4192A impedance analyzer with a bandwidth of 13.7 MHz. The AC oscillation amplitude was 400 mV$_{rms}$ for all figures in this letter. However, it should be noted that NC is observed for all investigated oscillation amplitudes between 50 mV$_{rms}$ and 500 mV$_{rms}$. All measurements were carried out in a nitrogen environment with <500 ppm H$_2$O at room temperature. Cole-Cole impedance plots of negative reactance versus resistance were generated from the impedance data taken at a range of driving frequencies (10–10^6 Hz).[20] Figure 1(a) shows a Cole-Cole impedance plot that is typical of the initial frequency dependent charge transport for an OLED biased at 10 V. The plot clearly arcs back toward the origin and possesses positive values of reactance, thus providing direct evidence of NC. The transient current in

---
[a)]Author to whom correspondence should be addressed; electronic mail: m-hersam@northwestern.edu
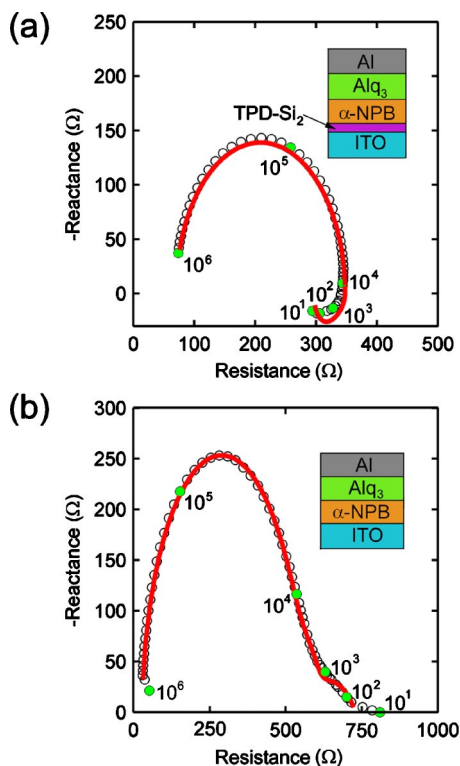
FIG. 1. (Color online) (a) Cole-Cole impedance plot for an OLED with TPD-Si$_2$ under an applied bias of 10 V (cross section illustrated in the inset). Evidence for NC is demonstrated by the low frequency arcing toward the origin (b) Cole-Cole impedance plot for an OLED fabricated without TPD-Si$_2$ under an applied bias of 28 V (cross section illustrated in the inset). In both plots, solid lines are fits that result from the equivalent circuit models shown in Fig. 3. The green data points were gathered at the noted frequencies in units of Hz.

response to a discontinuous change in the applied bias confirms the NC observed in the Cole-Cole impedance plot. In particular, following a step in the applied bias, the current initially peaks, then decreases due to geometrical device capacitance, and finally increases gradually due to NC. Figure 1(b) contains another Cole-Cole impedance plot taken on an OLED without the anode interfacial layer TPD-Si$_2$. As clearly evident in this plot, the NC behavior is overpowered by a low frequency capacitive tail.

Figure 2 illustrates the onset frequency of NC as a function of applied bias. The general trend of decreasing resistance and reactance with increasing bias has been previously reported[21] and is attributed to the increase in mobility with
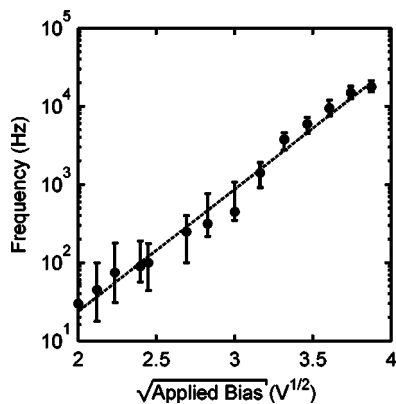

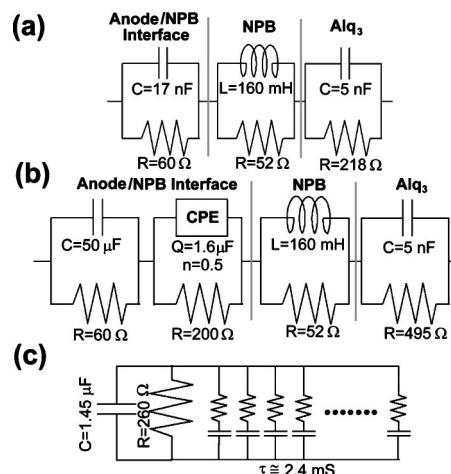FIG. 2. Onset frequency of NC plotted as a function of the square root of the applied bias.

FIG. 3. Schematic representation of the equivalent circuits used to model OLED behavior (a) with and (b) without the TPD-Si$_2$ interfacial layer. (c) Equivalent model for the anode-NPB interface without the TPD-Si$_2$ interfacial layer.

bias. To study this phenomenon quantitatively, the onset frequencies of NC are plotted as a function of applied bias. As seen in Fig. 2, the onset frequency of NC increases exponentially with the square root of the applied bias. This behavior correlates with Poole–Frenkel theory,[16] which states that the mobility in organic materials also increases exponentially with the square root of the applied bias.

Figures 3(a) and 3(b) are illustrations of the equivalent circuit models and values used to fit the observed frequency dependent charge transport. Figure 3(c) represents an equivalent model for the interface region of Fig. 3(b), which is more representative of the local physics. Parameters for the models were generated through the use of Equivalent Circuit[22] and optimized by minimizing the sum of the squared residual values.[23] Since the inductive behavior was not clearly demonstrated in the measurements of the device without TPD-Si$_2$, the values for the parallel resistor-inductor (RL) structure in the NPB layer were determined from the device containing TPD-Si$_2$ and then held constant in the model without the interfacial layer. The fits resulting from these equivalent circuit models have been overlaid on the data as solid lines in Fig. 1.

The equivalent circuit models can be correlated with the composition of the OLED heterostructure and thus provide insight into the physics of frequency dependent charge transport in these devices. Both equivalent circuit models [see Figs. 3(a) and 3(b)] contain a parallel resistor-capacitor (RC) element with R on the order of 100 Ω and C equal to 5 nF, which can be attributed to the Alq$_3$ electron transport layer. Due to the higher majority carrier mobility of NPB compared to Alq$_3$, holes accumulate in the device at the NPB-Alq$_3$ interface, thus effectively forming a parallel plate capacitor with the cathode.[21] In parallel with this capacitance is the field dependent resistance of Alq$_3$, which is expected to vary slightly between the two devices due to differences in the electrostatic potential distribution as a function of the composition of the OLED heterostructure. A calculation of the capacitance and resistance based upon the thickness, cross-sectional area, dielectric constant, and mobility of the Alq$_3$ layer yield R and C values that agree well with the optimized equivalent circuit models.[16]

To model the NPB layer and address NC, a parallel RL element is introduced [see Fig. 3(a) and 3(b)]. While the resistance matches expectations based upon the geometry and the mobility of the NPB layer, the mechanism for NC requires an analysis of transient space charge in the device. In response to a rapid increase in applied field, holes quickly traverse the NPB layer. However, once they reach the NPB/Alq$_3$ interface, the holes then await the arrival of electrons, which are delayed by both inefficient injection from the cathode prior to hole accumulation and the relatively low electron mobility in Alq$_3$. The delayed arrival of electrons leads to a temporary increase in the space charge, which prevents the injection of additional holes until the electrons arrive to relieve the space charge. This slow time constant feedback response leads to the apparent inductive behavior in OLED heterostructures and is similar in spirit to previously proposed models for NC.[15,24] In addition, the agreement with Poole–Frenkel theory (see Fig. 2) further illustrates that the feedback rate is dependent upon the transit time and, therefore, the mobility in the organics. The depression in the NC tail of Fig. 1(a) compared to the fit from the equivalent circuit model suggests a distribution in the carrier transit times across the Alq$_3$, which can be modeled as a constant phase element (CPE).[20]

The anode-NPB interface, when modified by TPD-Si$_2$, can be modeled by a lone parallel RC structure with a relatively fast time constant. The optimized values of $R=60$ Ω and $C=17$ nF [see Fig. 3(a)] correlate well with the TPD-Si$_2$ layer thickness of ~ 2 nm.[17] This interface can be modeled cleanly because TPD-Si$_2$ bonds with the underlying ITO layer as well as improving the surface energy match with the organics, thereby eliminating the slow time constant capacitive behavior that is characteristically observed without an interfacial layer. Consequently, at low frequencies, NC dominates for OLED heterostructures that contain TPD-Si$_2$ as observed in Fig. 1(a).

The anode interface without TPD-Si$_2$ requires a more complex model. For computational simplicity, the equivalent circuit model outlined in Fig. 3(b) was used to fit the data. However, this combination of R, C, and CPE elements can be transformed into the equivalent circuit of Fig. 3(c),[20] which is more illustrative of the physics of the interface. In Fig. 3(c), the parallel resistor describes the DC resistance of the interface, and the capacitance results from the ITO and the first available molecular state, which is located ~ 0.5 nm away.[25] A spacing of 0.5 nm implies a capacitance on the order of 1 μF, which is in agreement with the equivalent circuit model. In parallel with this interfacial resistance and capacitance is a distribution of additional RC elements shown in Fig. 3(c). Optimization of the equivalent circuit model in this case yields time constants for these additional RC elements that are approximately equal to 2.4 ms. Since trapping sites have time constants of this order of magnitude,[16] these RC elements are expected to be the circuit equivalent of a distributed set of interface traps. Sources of interface traps include unbonded hydroxyl groups on the ITO surface,[26,27] localized dewetting of the organic layers,[17,28] and the formation and fluctuation of local surface dipoles.[29,30] The net result of this slow capacitive time constant phenomenon is that NC is no longer directly observable

in the impedance spectra when TPD-Si$_2$ is removed from the OLED heterostructure [see Fig. 1(b)].

In conclusion, this letter has explored the role of NC in controlling frequency dependent charge transport in heterostructure OLEDs. In particular, when slow time constant interface trapping is quenched at the anode-organic interface with TPD-Si$_2$, NC dominates the device impedance at low frequencies. By studying the impedance spectra as a function of OLED heterostructure composition, equivalent circuit models have been developed that provide insight into the physical mechanisms of frequency dependent charge transport and suggest strategies for optimizing this behavior in display applications based on OLEDs.

[1]U. Mitschke and P. Bäuerle, J. Mater. Chem. **10**, 1471 (2000).
[2]T.-P. Nguyen and G. Horowitz, *Encyclopedia of Nanoscience and Nanotechnology* 7, 717 (American Scientific Publishers, Stevenson Ranch, California, 2004).
[3]eMagin, 2070 Route 52, Building 334, Hopewell Junction, NY 12533.
[4]W. E. Howard and O. F. Prache, IBM J. Res. Dev. **45**, 115 (2001).
[5]M. Matsumura and Y. Hirose, Appl. Surf. Sci. **175,176**, 740 (2001).
[6]N. A. Penin, Semiconductors **30**, 340 (1996).
[7]T. Misawa, J. Phys. Soc. Jpn. **12**, 882 (1957).
[8]S. E. Laux and K. Hess, IEEE Trans. Electron Devices **46**, 396 (1999).
[9]A. K. Jonscher, J. Chem. Soc., Faraday Trans. 2 **82**, 75 (1986).
[10]M. Ershov, H. C. Liu, L. Li, M. Buchanan, Z. R. Wasilewski, and V. Ryzhii, Appl. Phys. Lett. **70**, 1828 (1997).
[11]N. C. Chen, P. Y. Wang, and J. F. Chen, Appl. Phys. Lett. **72**, 1081 (1998).
[12]G. B. Parravicini, A. Stella, M. C. Ungureanu, and R. Kofman, Appl. Phys. Lett. **85**, 302 (2004).
[13]H. L. Kwok, Solid-State Electron. **47**, 1089 (2003).
[14]I. N. Hulea, R. F. J. van der Scheer, H. B. Brom, B. M. W. Langeveld-Voss, A. van Dijken, and K. Brunner, Appl. Phys. Lett. **83**, 1246 (2003).
[15]V. R. Nikitenko, Y.-H. Tak and H. Bässler, J. Appl. Phys. **84**, 2334 (1998).
[16]W. Brütting, H. Riel, T. Beierlein, and W. Riess, J. Appl. Phys. **89**, 1704 (2001).
[17]J. Cui, Q. Huang, J. C. G. Veinot, H. Yan, Q. Wang, G. R. Hutchison, A. G. Richter, G. Evmenenko, P. Dutta, and T. J. Marks, Langmuir **18**, 9958 (2002).
[18]T. Yamamoto, M. Nighiyama, and Y. Koie, Tetrahedron Lett. **39**, 2367 (1998).
[19]M. Hiramoto, T. Miyao, and M. Yokoyama, Appl. Phys. Lett. **57**, 1625 (1990).
[20]J. R. Macdonald, *Impedance Spectroscopy* (Wiley, New York, 1987).
[21]C. Jonda and A. B. R. Mayer, Chem. Mater. **11**, 2429 (1999).
[22]B. A. Boukamp, University of Twente, the Netherlands (1989).
[23]G. E. P. Box, W. G. Hunter, and J. S. Hunter, *Statistics for Experiments* (Wiley, New York, 1978).
[24]D. V. Khramtchenkov, V. I. Arkhipov, and H. Bässler, J. Appl. Phys. **81**, 6954 (1997).
[25]V. I. Arkhipov, E. V. Emelianova, Y. H. Tak, and H. Bässler, J. Appl. Phys. **84**, 848 (1998).
[26]C. Donley, D. Dunphy, D. Paine, C. Carter, K. Nebesny, P. Lee, D. Alloway, and N. R. Armstrong, Langmuir **18**, 450 (2002).
[27]K.-J. King and O. Kim, J. Electrochem. Soc. **144**, 2501 (1997).
[28]M. Hiramoto, K. Nakayama, I. Sato, H. Kumaoka, and M. Yokoyama, Thin Solid Films **331**, 71 (1998).
[29]F. Nuesch, E. W. Forsythe, Q. T. Lee, Y. Gao, and L. J. Rothberg, J. Appl. Phys. **87**, 7973 (2000).
[30]A. Kahn, N. Koch, and W. Gao, J. Polym. Sci., Part B: Polym. Phys. **41**, 2529 (2003).